Ion Transport in Cryptand and Crown Ether Lithium Salt Complexes

Rensl E. A. Dillon and Duward F. Shriver*

Department of Chemistry and Materials Research Center, Northwestern University, Evanston, Illinois, 60208-3113

Received June 11, 1999. Revised Manuscript Received September 1, 1999

Amorphous solid electrolytes were formed by the interaction of cryptands or crown ethers with a lithium salt, $Li[CF_3SO_2N(CH_2)_3OCH_3]$, when the cavity size of the macrocycle does not match the diameter of the lithium cation. With the exception of $[Li\subset 18\text{-C-}6][(CF_3SO_2)_2N]$ (the mathematical symbol of inclusion, $\subset$, is used to indicate Li^+ included in 18-C-6), the complexes of $Li[(CF_3SO_2)_2N]$ with cryptand and crown ethers do not form amorphous electrolytes. Complexes of $Li[CF_3SO_2N(CH_2)_3OCH_3]$ and $Li[(CF_3SO_2)_2N]$ were examined by thermal, spectroscopic, and conductivity methods to determine the role of the anion on ionic glass formation.

Introduction

Solid polymer electrolytes have attracted considerable attention for application in solid-state electrochemical devices, including high-energy-density batteries.[1−3] These materials consist of a solid polymer host and an alkali-metal salt which is solvated by the polar moieties in the polymer. Unlike crystalline or glassy solid electrolytes, polymer electrolytes can be formulated as compliant materials that can deform to accommodate the volume changes that typically occur in the charge/discharge cycles of rechargeable batteries.

Ion transport in semicrystalline complexes of alkali-metal salts in poly(ethylene oxide) (PEO) was originally thought to occur via ion hopping along the interior of the crystalline PEO helix.[4] However, Berthier and co-workers clearly demonstrated, using NMR measurements, that ionic mobility primarily occurs in the amorphous regions of the electrolyte.[5] This result led to a model of cooperative ion−polymer motion for ion transport. The concept that ion motion is coupled to the structural relaxations of the polymer is supported by evidence such as the poor conductivity of the electrolyte below the glass transition temperature, where the segmental motion of the polymer is largely frozen. These ideas prompted the synthesis of fully amorphous polar polymers that have glass transitions well below room temperature. For example, poly[(bis(2(2-methoxyethoxy)ethoxy)phosphazene] (MEEP) consists of a highly flexible poly(phosphazene) backbone with short polyether side chains, a combination that results in a low glass transition of approximately −80 °C.[6] The complexes of MEEP with the lithium salt $LiCF_3SO_3$ have substantially higher ionic conductivities than those of $LiCF_3SO_3$−PEO complexes.[7]

The dissolution of a salt into a polymer occurs when the free energy gain upon solvation is sufficiently favorable to overcome the lattice energy of the salt. Therefore, alkali-metal salts, with bulky, charge-delocalized anions and attendant low lattice energies, readily form polymer salt complexes. Research on these types of ionic conductors has evolved from polar polymers containing relatively simple salts such as $LiBF_4$, $LiCF_3SO_3$, and LiI, to salts with larger and less basic anions, such as $Li[(CF_3SO_2)_2N]$, $Li[(CF_3SO_2)_3C]$, and $Li[(C_4F_9SO_2)_2N]$. The large mononegative anions in the latter group suppress ion pairing and thereby improve the ionic conductivity in the low dielectric medium of the polymer host. For example, the PEO complexes of $Li[(CF_3SO_2)_2N]$ exhibit a higher ionic conductivity than that of $LiCF_3SO_3$−PEO complexes.[8] The lower ionic conductivity for the $LiCF_3SO_3$−PEO complexes is attributed to the greater tendency of $LiCF_3SO_3$ to form ion pairs. An added benefit of salts with large anions is their resistance to form crystalline PEO complexes, hence the name plasticizing salts. Amorphous complexes generally exhibit higher ionic conductivity than their crystalline counterparts.[9]

Recent variations in polymer electrolytes include the following: (a) plasticized polymer electrolytes or gel electrolytes which are polymer salt complexes doped with low molecular weight polar or ion chelating additives,[10−13] (b) composite electrolytes made up of

(1) Ratner, M. A.; Shriver, D. F. *Chem. Rev.* **1988**, *88*, 109.
(2) Armand, M. B.; Chabagno, J. M.; Duclot, M. J. In *Fast Ion Transport in Solids Electrodes and Electrolytes*; Vashishta, P., Mundy, J. N., Shenoy, G. K., Eds.; Elsevier North-Holland, Inc.: Lake Geneva, IL, 1979.
(3) Julien, C.; Nazri, G. *Solid State Batteries: Materials Design and Optimization*; Kluwer Academic Publishers: Boston, MA, 1994.
(4) Dupon, R.; Papke, B. L.; Ratner, M. A.; Whitmore, D. H.; Shriver, D. F. *J. Am. Chem. Soc.* **1982**, *104*, 6247.
(5) Berthier, C.; Gorecki, W.; Minier, M.; Armand, M. B.; Chabagno, J. M.; Rigaud, P. *Solid State Ionics* **1983**, *11*, 91.
(6) Blonsky, P. M.; Shriver, D. F.; Austin, P.; Allcock, H. R. *J. Am. Chem. Soc.* **1984**, *106*, 6854.
(7) Blonsky, P. M.; Shriver, D. F.; Austin, P.; Allcock, H. R. *Solid State Ionics* **1986**, *18−19*, 258.
(8) Vallee, A.; Besner, S.; Prud'homme, J. *Electrochim. Acta.* **1992**, *37*, 1579.
(9) Armand, M. *Solid State Ionics* **1994**, *69*, 309.
(10) Xia, D. W.; Soltz, D.; Smid, J. *Solid State Ionics* **1984**, *14*, 221.
(11) Abraham, K. M.; Alamgir, M. *J. Electrochem. Soc.* **1990**, *137*, 1657.

10.1021/cm990376f CCC: $18.00
Published on Web 10/27/1999

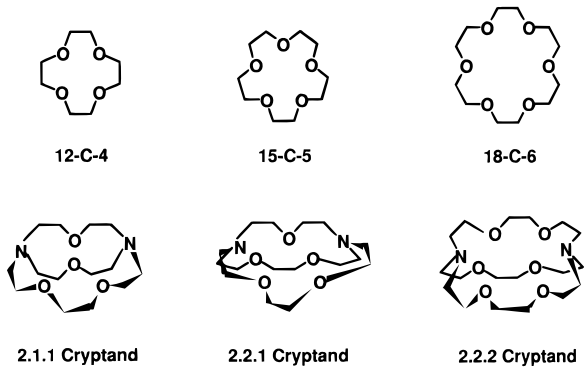

Figure 1. Crown ether and cryptand macrocycles.

plasticized polymer electrolytes or gel electrolytes doped with inorganic fillers such as Al_2O_3,[14] γ-$LiAlO_2$[15] and SiO_2[16] and (c) "rubbery electrolytes" (also called "polymer-in-salt" electrolytes), which are supercooled mixtures of lithium salts doped with PEO.[17,18] Related ionically conductive systems include the following: (a) ionic liquids formed by complex formation between lithium salts and Lewis acids,[19,20] (b) low-temperature molten salts such as alkylpyridinium or alkylimidazolium organic cation,[21−23] and (c) "inorganic salt−organic salt" hybrid systems that combine a polyelectrolyte and a salt to achieve an ionically conducting amorphous electrolyte.[24,25] The features that generally provide electrolytes with good ionic conductivity are weak ion pairing and an amorphous or semiliquid state for the electrolyte.[26]

In this investigation we explored the role of the anion in the formation of amorphous ionically conducting electrolyte complexes. We have reported preliminary results for cryptand and crown ethers with $Li[CF_3SO_2N(CH_2)_3OCH_3]$.[27] In the present work, we explore electrolytes based on $Li[(CF_3SO_2)_2N]$, where the charge on the anion is highly delocalized. This anion appears to interact more weakly than $[CF_3SO_2N(CH_2)_3OCH_3]^-$ with the lithium cation.

Cryptands and crown ethers, Figure 1, exhibit size selectivity for cations, and Table 1 provides the cavity radii of the crown ethers and cryptands used in this study.[28] Given a choice between the 12-C-4 and 18-C-6 crown ethers, a lithium cation will choose the smaller 12-C-4 crown ether, because a stronger complex results when the ionic radius of the cation ($Li^+ \approx 0.8$ Å, Table 1) matches the cavity radius of the crown ether (12-C-4 $\approx$ 0.77 Å). The three-dimensional cryptands wrap around a cation, resulting in higher binding constants than for comparable crown ethers.[29] Generally, the binding constant for a cryptand complex, [Li⊂2.1.1][X] (2.1.1 is equivalent to 2.1.1-cryptand) is about 10^5 greater than that of the [Li⊂12-C-4][X] complex, where X is a simple anion such as I^-.[30−32] The binding constant of the cryptand or crown ether will play an important role in the properties of the resulting complex.

Table 1. Approximate Cavity Radii of Cation Encapsulating Macrocycles and Ionic Radii of Alkali-Metal Cations[a]

macrocycle	cavity radius (Å)	cation	ionic radius (Å)
12-C-4	0.72−0.81	Li^+	0.74−0.86
15-C-5	0.86−1.10	Na^+	0.95−1.12
18-C-6	1.34−1.43	K^+	1.33−1.44
2.1.1 cryptand	0.75−0.84		
2.2.1 cryptand	1.00−1.25		
2.2.2 cryptand	1.35−1.40		

[a] From X-ray crystallographic data and Corey-Pauling-Koltun models.[28]

Variations in the size of a cation influence the melting point of a salt system. For example, $Li[CF_3SO_2N(CH_2)_3OCH_3]$ has a melting point of 256 °C and $K[CF_3SO_2N(CH_2)_3OCH_3]$ melts at 45 °C, with an attendant low glass transition temperature of −9 °C.[33] $Li[(CF_3SO_2)_2N]$ and $K[(CF_3SO_2)_2N]$ melt at 234 and 205 °C, respectively.[33] The melting points of the lithium and potassium salts of the $[CF_3SO_2N(CH_2)_3OCH_3]^-$ and $[(CF_3SO_2)_2N]^-$ indicate that cation size (Table 1) significantly influences the melting points of $[CF_3SO_2N(CH_2)_3OCH_3]^-$ salts but not those of the corresponding $[(CF_3SO_2)_2N]^-$ salts. Similarly, the size of [Li⊂cryptand]$^+$ and [Li⊂crown ether]$^+$ cations influences the properties of the salt macrocycle complexes.

Experiment

Materials. Experimental manipulations were carried out under an inert atmosphere of dry nitrogen. $Li[CF_3SO_2N(CH_2)_3OCH_3]$ was prepared as previously described, and the reported ^{1}H NMR and the melting point agreed with the literature values.[33] The identity of this material was also verified by FAB$^-$, FTIR, elemental analysis, and ^{19}F NMR data. $Li[(CF_3SO_2)_2N]$ (3M) was dried on a high vacuum line at 150 °C for 2 days (8×10^{-6} Torr) and then handled in a drybox. All macrocycles were purchased from Aldrich. The crown ethers, 12-C-4 and 15-C-5, were dried over molecular sieves for more than 48 h, and 18-C-6 was sublimed at 35 °C (1×10^{-1} Torr). 2.2.2-Cryptand was dried on a high vacuum line at 30 °C (8×10^{-6} Torr), and samples of 2.2.1-cryptand and 2.1.1-cryptand, supplied in sealed ampules, were used as received. Tetrahy-

(12) Choe, H. S.; Carroll, B. G.; Pasquariello, D. M.; Abraham, K. M. *Chem. Mater.* **1997**, *9*, 369.
(13) Ballard, D. G. H.; Cheshire, P.; Mann, T. S.; Przeworski, J. E. *Macromolecules* **1990**, *23*, 1256.
(14) Nagasubramanian, G.; Attia, A. I.; Halpert, G.; Peled, E. *Solid State Ionics* **1993**, *67*, 51.
(15) Appetecchi, G. B.; Croce, F.; Dautzenberg, G.; Mastragostino, M.; Ronci, F.; Scrosati, B.; Soavi, F.; Zanelli, A.; Alessandrini, F.; Prosini, P. P. *J. Electrochem. Soc.* **1998**, *145*, 4126.
(16) Fan, J.; Fedkiw, P. S. *J. Electrochem. Soc.* **1997**, *144*, 399.
(17) Angell, C. A.; Liu, C.; Sanchez, E. *Nature* **1993**, *362*, 137.
(18) Angell, C. A.; Fan, J.; Liu, C.; Lu, Q.; Sanchez, E.; Xu, K. *Solid State Ionics* **1994**, *69*, 343.
(19) Liu, C.; Angell, C. A. *Solid State Ionics* **1996**, *86−88*, 467.
(20) Liu, C.; Teeters, D.; Potter, W.; Tapp, B.; Sukkar, M. H. *Solid State Ionics* **1996**, *86−88*, 431.
(21) Watanabe, M.; Yamada, S.; Ogata, N. *Electrochim. Acta* **1995**, *40*, 2285.
(22) Fuller, J.; Carlin, R. T.; De Long, H. C.; Haworth, D. *J. Chem. Soc., Chem. Commun.* **1994**, 299.
(23) Bonhote, P.; Dias, A.; Papageorgiou, N.; Kalyanasundaram, K.; Gratzel, M. *Inorg. Chem.* **1996**, *35*, 1168−1178.
(24) Hu, S.; Fang, S. *Electrochim. Acta* **1999**, *44*, 2721.
(25) Ito, K.; Ohno, H. *Electrochim. Acta* **1998**, *43*, 1247.
(26) Angell, C. A.; Xu, K.; Zhang, S.; Videa, M. *Solid State Ionics* **1996**, *86−88*, 17.
(27) Dillon, R. E.; Shriver, D. F. In *Materials Research Society*; Ginley, D. S., Doughty, D. H., Scrosati, B., Takamura, T., Zhang, Z., Eds.; Materials Research Society: Boston, MA, 1998; Vol. 496.
(28) Izatt, R. M.; Bradshaw, J. S.; Nielsen, S. A.; Lamb, J. D.; Christensen, J. J. *Chem. Rev.* **1985**, *85*, 271.
(29) Lindoy, L. F. *The Chemistry of Macrocyclic Ligand Complexes*; Cambridge University Press: Cambridge, England, 1989.
(30) Lehn, J. M.; Sauvage, J. P. *J. Am. Chem. Soc.* **1975**, *97*, 6699.
(31) Lamb, J. D.; Izatt, R. M.; Swain, C. S.; Christensen, J. J. *J. Am. Chem. Soc.* **1980**, *102*, 475.
(32) Michaux, G.; Reisse, J. *J. Am. Chem. Soc.* **1982**, *104*, 6895.
(33) Lascaud, S.; Perrier, M.; Vallee, A.; Besner, S.; Prud'homme, J.; Armand, M. *Macromolecules* **1994**, *27*, 7469.

Table 2. DSC Data of $Li[CF_3SO_2N(CH_2)_3OCH_3]$ in a 1:1 Ratio with Various Cation Encapsulating Macrocycles[a]

complex	T_g	T_m	T_g*	T_c*	T_m*
[Li⊂12-C-4]		97	−18	44	94
[Li⊂15-C-5]	−26				
[Li⊂18-C-6]	−31				
[Li⊂2.1.1]		66	−35		
[Li⊂2.2.1]	−57				
[Li⊂2.2.2]	−50				

[a] Key: T_g (°C), glass transition temperature; T_g* (°C), glass transition temperature after quenching; T_m (°C), melting temperature; T_m* (°C), melting temperature after quenching; T_c (°C), cold crystallization temperature; T_c* (°C), cold crystallization temperature after quenching.

Table 3. DSC Data of $Li[(CF_3SO_2)_2N]$ in a 1:1 Ratio with Various Cation Encapsulating Macrocycles[a]

complex	T_g	T_m	T_g*	T_c*	T_m*
[Li⊂12-C-4]		61, 109			97
[Li⊂15-C-5]		83	−44	4	66,79
[Li⊂18-C-6]	−53	36	−50	−19	29
[Li⊂2.1.1]		72	−31	31	61
[Li⊂2.2.1]		26, 135			25,132
[Li⊂2.2.2]		61, 129		29	61, 126

[a] Key: T_g (°C), glass transition temperature; T_g* (°C), glass transition temperature after quenching; T_m (°C), melting temperature; T_m* (°C), melting temperature after quenching; T_c (°C), cold crystallization temperature; T_c* (°C), cold crystallization temperature after quenching.

drofuran (THF) was distilled under nitrogen from sodium benzophenone.

Complex Formation. Complexes of the salts $Li[CF_3SO_2N(CH_2)_3OCH_3]$ and $Li[(CF_3SO_2)_2N]$ were prepared by adding THF to equimolar quantities of the salt and a macrocycle. After formation of a homogeneous solution, the solvent was removed under vacuum at 50 °C (1×10^{-1} Torr) for a day, followed by 40 °C (8×10^{-6} Torr) for 2 days. Samples were free of residual solvent and water as judged by infrared spectroscopy and they were stored in a dry inert atmosphere.

Physical Characterization. Differential scanning calorimetry (DSC) was performed on a Perkin-Elmer Pyris 1 instrument on samples loaded in hermetically sealed aluminum pans. A stable baseline was observed over the temperature range −100 to +200 °C, and the instrument was calibrated using indium and decane. All transitions were recorded at a heating rate of 40 °C/min. Glass transitions were assigned at the middle of the transition. Melting and cold crystallization temperatures were assigned to the onset of the transitions. Amorphous materials exhibited a glass transition as the only thermal transition in the first DSC scan (not melt quenched). Crystalline samples were melted and subsequently quenched to −100 °C at 200 °C/min in an attempt to form amorphous materials. The DSC scan after quenching was used to detect the following transitions: T_c (cold crystallization), T_g* (glass transition after quenching), and T_m* (melting point after quenching).

Raman spectra were recorded on a FT-Raman spectrometer with excitation by a Nd:YAG laser at 1.064 μm. All samples were placed in capillary tubes and probed in a 180° backscattered geometry. Amorphous samples exhibited weaker and broader bands in comparison to the sharper spectra of crystalline samples. The spectral resolution of the interferometer was 4 cm^{-1}. Infrared spectra were recorded on a Bomem MB-100 FTIR spectrometer at 2 cm^{-1} resolution. Amorphous samples were placed between KBr plates and transferred under N_2. Crystalline samples were prepared as KBr pellets.

Complex impedance measurements were performed with a Hewlett-Packard 4192A in the frequency range 5 Hz to 13 MHz, on samples sandwiched between stainless steel electrodes and annealed for 12−24 h at 100 °C before data collection. Data were collected at ∼10 °C intervals as samples were cycled between 100 and 20 °C using a temperature ramp of 0.2 °C/min.

Results

Thermal Properties of the $Li[CF_3SO_2N(CH_2)_3OCH_3]$ and $Li[(CF_3SO_2)_2N]$ Complexes. Izatt and coworkers found that the most stable salt−macrocycle complexes are formed when the cation diameter matches the size of the macrocycle cavity.[28] The lithium cation matches the macrocycle cavities of 12-C-4 and 2.1.1-cryptand, and the DSC data in Table 2 show that both macrocycles form crystalline complexes with $Li[CF_3SO_2N(CH_2)_3OCH_3]$. In general, cryptands reduce ion pairing more effectively than their related crown ether macrocycles and this trend correlates with the result that the $[Li⊂2.1.1][CF_3SO_2N(CH_2)_3OCH_3]$ complex has a lower melting point than that of $[Li⊂12\text{-}C\text{-}4][CF_3SO_2N(CH_2)_3OCH_3]$. The melt was quenched on the DSC instrument to produce an amorphous phase for both the 12-C-4 and 2.1.1-cryptand complexes. When the quenched sample is heated $[Li⊂12\text{-}C\text{-}4][CF_3SO_2N(CH_2)_3OCH_3]$ undergoes cold crystallization; by contrast, $[Li⊂2.1.1][CF_3SO_2N(CH_2)_3OCH_3]$ remained amorphous.

The amorphous phase, observed for $Li[CF_3SO_2N(CH_2)_3OCH_3]$ complexes with either 15-C-5 or 18-C-6, appears to originate from the disparity between the cavity size of the crown ethers and the lithium cation radius. Similarly, amorphous materials are observed for complexes of $Li[CF_3SO_2N(CH_2)_3OCH_3]$ with 2.2.1-cryptand and 2.2.2-cryptand. The lower glass transition temperatures of the cryptand complexes compared with the crown ether analogues may result from the reduced Coulombic cation−anion interaction for the cryptand system, where the cation is surrounded on all sides by the three-dimensional cryptand ligand.

Thermal properties of the $Li[(CF_3SO_2)_2N]$ macrocycle complexes, Table 3, indicate crystalline materials, with the exception of $[Li⊂18\text{-}C\text{-}6][(CF_3SO_2)_2N]$. These crystalline complexes exhibit multiple melting points both before and after quenching, suggesting that several different phases are present.

As noted in the Introduction, the size of the cation significantly changes the melting points of the $[CF_3SO_2N(CH_2)_3OCH_3]^-$ salts. Similarly, $Li[CF_3SO_2N(CH_2)_3OCH_3]$ complexes are observed to have significantly different thermal properties when the size of the [Li⊂macrocycle] cation varies. For example, the $[Li⊂12\text{-}C\text{-}4][CF_3SO_2N(CH_2)_3OCH_3]$ complex is crystalline (T_m = 97 °C) and the $[Li⊂18\text{-}C\text{-}6]$ $[CF_3SO_2N(CH_2)_3OCH_3]$ complex is amorphous (T_g = −31 °C). Comparisons between $Li[(CF_3SO_2)_2N]$ (T_m = 234 °C) and $K[(CF_3SO_2)_2N]$ (T_m = 205 °C) indicate that cation size has a modest influence on the melting point of the $[(CF_3SO_2)_2N]^-$ salts. Similarly, $Li[(CF_3SO_2)_2N]$ cryptand and crown ether complexes have comparable thermal properties. These observations suggest that the influence of cation size on $Li[CF_3SO_2N(CH_2)_3OCH_3]$ and $Li[(CF_3SO_2)_2N]$ is maintained for the analogous cryptand and crown ether complexes.

Raman Spectroscopic Analysis of the Anion Modes on Complexation. Upon addition of a macrocycle to $Li[(CF_3SO_2)_2N]$ or $Li[CF_3SO_2N(CH_2)_3OCH_3]$ a new band at ∼860 cm^{-1} is observed (Table 4). This band was originally attributed to a symmetric ring breathing motion of crown ether oxygens surrounding solvated

Table 4.. Raman Frequencies and Vibrational Assignments for Li[$(CF_3SO_2)_2N$] (LiTFSI), Li[$CF_3SO_2N(CH_2)_3OCH_3$] (LiMPSA), and Macrocycle Complexes (700−1550 cm^{-1})[a]

assignment	LiTFSI	A	B	C	D	E	F
$\nu_s(CF_3)$ (s)	1247	1241	1244	1243	1241	1242	1243
$\nu_s(SO_2)$ (m)	1131	1138	1138	1140	1141	1139	1145
$\nu_{srb}(CH_2-O)$ (s)		862	876	860	849	848	852
$\delta_s(CF_3)$ (vs)	747	746, 741	741	742	742	740	740

assignment	LiMPSA	G	H	I	J	K	L
$\nu_{srb}(CH_2-O)$ (s)		863	872	864	849	851	846
$\delta_s(CF_3)$ (vs)	750	745	746	746	739	738	738

[a] Assignments: ν (stretching); δ (bending). The subscripts s and srb denote symmetric and symmetric ring breathing motions, respectively. Band intensities: vs (very strong); s (strong); m (medium).Key: (A) [Li⊂12-C-4][$(CF_3SO_2)_2N$]; (B) [Li⊂15-C-5][$(CF_3SO_2)_2N$]; (C) [Li⊂18-C-6][$(CF_3SO_2)_2N$]; (D) [Li⊂2.1.1][$(CF_3SO_2)_2N$]; (E) [Li⊂2.2.1][$(CF_3SO_2)_2N$]; (F) [Li⊂2.2.2][$(CF_3SO_2)_2N$]; (G) [Li⊂12-C-4][$CF_3SO_2N(CH_2)_3OCH_3$]; (H) [Li⊂15-C-5][$CF_3SO_2N(CH_2)_3OCH_3$]; (I) [Li⊂18-C-6][$CF_3SO_2N(CH_2)_3OCH_3$]; (J) [Li⊂2.1.1][$CF_3SO_2N(CH_2)_3OCH_3$]; (K) [Li⊂2.2.1][$CF_3SO_2N(CH_2)_3OCH_3$]; (L) [Li⊂2.2.2][$CF_3SO_2N(CH_2)_3OCH_3$].

cations.[34] Similar bands were reported by Papke in polymer salt complexes and assigned to a combination of ring breathing and CH_2 rocking modes of the host polymer.[35] More recently, Frech and Huang determined the spectra of salt complexes with deuterated diglyme and they suggest that the intense band at ∼860 cm^{-1} is primarily a CH_2 rocking vibration.[36] Whatever the origin, it is clear that the 860 cm^{-1} band is associated with complexation. This band shifts to lower wavenumbers, ∼850 cm^{-1}, for the Li[$(CF_3SO_2)_2N$] and [Li][$CF_3SO_2N(CH_2)_3OCH_3$] cryptand complexes. Doan and co-workers have reported similar results for [Na⊂2.2.2] complexes.[37]

The strongest band in the Raman spectra of Li[$(CF_3SO_2)_2N$], and of Li[$CF_3SO_2N(CH_2)_3OCH_3$] are assigned as a symmetric deformation mode, $\delta_s(CF_3)$, at 747 and 750 cm^{-1} respectively.[38] Li[$(CF_3SO_2)_2N$] complexes exhibit the $\delta_s(CF_3)$ band at lower wavenumbers (∼741 cm^{-1}), and this frequency is similar to that observed by Rey and co-workers for free $[(CF_3SO_2)_2N]^-$ in Li[$(CF_3SO_2)_2N$]−PEO complexes.[39,40] Cryptand and crown macrocycles appear to have a similar effect on the environment of $[(CF_3SO_2)_2N]^-$ despite their different affinities for the lithium cation. This result suggests that ion pairing in Li[$(CF_3SO_2)_2N$] is weak and that both crown ethers and cryptands lead to complexes with "free ions". The $\delta_s(CF_3)$ bands in [Li⊂cryptand][$CF_3SO_2N(CH_2)_3OCH_3$] complexes are shifted to lower frequency (∼738 cm^{-1}) than for the corresponding [Li⊂crown ether][$CF_3SO_2N(CH_2)_3OCH_3$] complexes (∼746 cm^{-1}), Figure 2. The difference in $\delta_s(CF_3)$ bands for Li[$CF_3SO_2N(CH_2)_3OCH_3$] cryptand and crown ether complexes confirm that coordination of the lithium by cryptand macrocycles

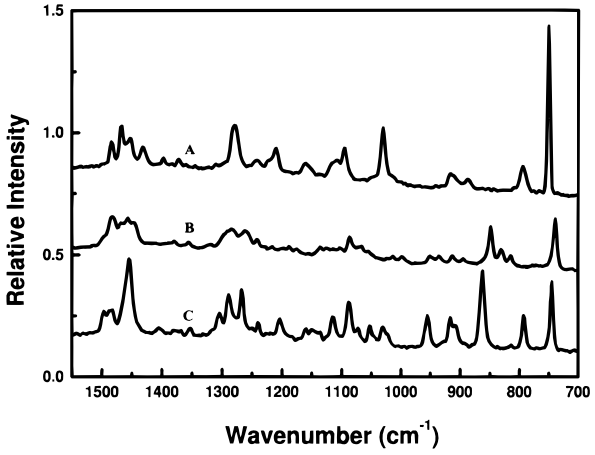

Figure 2. Representative Raman spectra for Li[$CF_3SO_2N(CH_2)_3OCH_3$] macrocycle complexes: (A) Li[$CF_3SO_2N(CH_2)_3OCH_3$]; (B) [Li⊂2.1.1][$CF_3SO_2N(CH_2)_3OCH_3$]; (C) [Li⊂12-C-4][$CF_3SO_2N(CH_2)_3OCH_3$].

exerts a greater influence than lithium coordination to crown ethers.

FTIR Investigation of Anion−Cation Interactions. As shown in Tables 5 and 6, the $\nu_{as}(SO_2)$ and $\nu_s(SO_2)$ bands differ for Li[$(CF_3SO_2)_2N$] and Li[$CF_3SO_2N(CH_2)_3OCH_3$], and the origin of this difference becomes evident upon examination of the crystal structures of these salts. For Li[$(CF_3SO_2)_2N$], the lithium cation is coordinated tetrahedrally by four oxygens from four different anions, whereas the lithium cation in Li[$CF_3SO_2N(CH_2)_3OCH_3$] is four coordinate via SO oxygens from two different anions and, an etheric oxygen and nitrogen atom from a third anion.[41,42] Complex formation between Li[$(CF_3SO_2)_2N$] and 12-C-4 results in a split of the $\nu_{as}(SO_2)$ band, with the major peak moving to 1360 cm^{-1} and a weaker band remaining at 1335 cm^{-1} (Figure 3).[40] A less dramatic change from 1151 to 1140 cm^{-1} occurs in the $\nu_s(SO_2)$ band upon complexation with 12-C-4. The [Li⊂12-C-4][$CF_3SO_2N(CH_2)_3OCH_3$] complex exhibits a major change in the $\nu_s(SO_2)$ band (from 1164 to 1139 cm^{-1}) and a minor shift in the $\nu_{as}(SO_2)$ band (from 1277 to 1289 cm^{-1}). The [Li⊂12-C-4][$(CF_3SO_2)_2N$] and [Li⊂12-C-4][$CF_3SO_2N(CH_2)_3OCH_3$] complexes feature $\nu_s(SO_2)$ bands in approximately the same position but the $\nu_{as}(SO_2)$ bands differ significantly.

FTIR spectra confirm the observations made in the Raman study, that cryptand and crown macrocycles perturb the $[(CF_3SO_2)_2N]^-$ modes equally, as indicated by the similarity of the $\nu_{as}(SO_2)$ and $\nu_s(SO_2)$ bands. FTIR spectra also correlate with the thermal properties of the [Li⊂macrocycle][$(CF_3SO_2)_2N$] complexes which display multiple melting points and also display multiple peak splitting, as indicated by $\nu_{as}(C-O-C)$ bands. For example, the crystal structure of [Li⊂2.2.2][$(CF_3SO_2)_2N$][43] shows that the lithium cation is coordinated to four of the six etheric oxygens in the macrocycle, resulting in coordinated and uncoordinated $\nu_{as}(C-O-C)$ bands. In general, [Li⊂macrocycle][$(CF_3SO_2)_2N$] complexes pos-

(34) Sato, H.; Kusumoto, Y. *Chem. Lett.* **1978**, 635.
(35) Papke, B. L.; Ratner, M. A.; Shriver, D. F. *J. Phys. Chem. Solids* **1981**, *42*, 493.
(36) Frech, R.; Huang, W. *Macromolecules* **1995**, *28*, 1246.
(37) Doan, K. E.; Heyen, B. J.; Ratner, M. A.; Shriver, D. F. *Chem. Mater.* **1990**, *2*, 539.
(38) Ferry, A.; Doeff, M. M.; De Jonghe, L. C. *J. Electrochem. Soc.* **1998**, *145*, 1586.
(39) Rey, I.; Lassegues, J. C.; Grondin, J.; Servant, L. *Electrochim. Acta* **1998**, *43*, 1505.
(40) Rey, I.; Johansson, P.; Lindgren, J.; Lassegues, J. C.; Grondin, J.; Servant, L. *J. Phys. Chem.* **1998**, *102*, 3249.
(41) Nowinski, J. L.; Lightfoot, P.; Bruce, P. G. *J. Mater. Chem.* **1994**, *4*, 1579.
(42) Dillon, R. E.; Stern, C. L.; Shriver, D. F. Manuscript in preparation.
(43) Dillon, R. E.; Shriver, D. F. To be published.

Table 5. FTIR Frequencies and Vibrational Assignments for Li[$(CF_3SO_2)_2N$] (LiTFSI) and Macrocycle Complexes (400−1450 cm^{-1})[a]

assignment	LiTFSI	A	B	C	D	E	F
$\nu_{as}(SO_2)$ (s−m)*	1335	1360, 1336	1358, 1335	1349	1355, 1335	1355, 1336	1357, 1337
$\nu_s(CF_3)$ (sh)	1246			1234			
$\nu_{as}(CF_3)$ (s)	1208	1203	1226, 1198	1193	1227, 1206	1227, 1195	1226, 1202, 1184
$\nu_s(SO_2)$ (m)	1151	1140	1139	1135	1136, 1121	1139	1146, 1136
ν_{as}(COC) (s)		1098, 1085	1115	1110, 1086	1104, 1083	1104	1117, 1106, 1094, 1083
ν_{as}(SNS) (m)	1083, 1068	1055	1059	1060	1065, 1049	1058	1056
$\delta_{as}(SO_2)$ (m)	644	618	617	616	617	618	612
$\delta_{as}(CF_3)$ (w)	575	574	570	580, 571	570	570	570
$\delta_{as}(CF_3)$ (w)	516	519	515	514	515	514	515

[a] Assignments: ν (stretch); δ (bend). Subscripts ***as*** and ***s*** denote asymmetric and symmetric motions, respectively. Band intensities: s (strong); s−m (strong to medium); m (medium); w (weak). *$\nu_{as}(SO_2)$ (s) splits into two peaks, and the weaker band is at a lower wavenumber. Key: (A) [Li⊂12-C-4][$(CF_3SO_2)_2N$]; (B) [Li⊂15-C-5][$(CF_3SO_2)_2N$]; (C) [Li⊂18-C-6][$(CF_3SO_2)_2N$]; (D) [Li⊂2.1.1][$(CF_3SO_2)_2N$]; (E) [Li⊂2.2.1][$(CF_3SO_2)_2N$]; (F) [Li⊂2.2.2][$(CF_3SO_2)_2N$]

Table 6. . FTIR Frequencies and Vibrational Assignments for Li[$CF_3SO_2N(CH_2)_3OCH_3$] (LiMPSA) and Macrocycle Complexes (400−1450 cm^{-1})[a]

assignment	LiMPSA	G	H	I	J	K	L
$\nu_{as}(SO_2)$ (s)	1277	1289	1280	1280	1265	1263	1285, 1264
$\nu_s(CF_3)$ (m)	1246	1250	1242	1242	1238		1238
$\nu_{as}(CF_3)$ (s)	1211	1200	1203	1205	1196	1194	1196
$\nu_s(SO_2)$ (m)	1164	1139					
ν_{as}(COC) (s)	1106, 1091	1111, 1089	1115	1109	1108	1109	1107
ν_{as}(CNS) (w)	1048	1046	1047	1046		1031	
$r_{as}(CH_2)$ (w)	1024	1022	1020	1020			
$\delta_{as}(SO_2)$ (m)	622	627	609	611	608	609	609

[a] Assignments: ν (stretch); r (rock); δ (bend). Subscripts as and s denote asymmetric and symmetric motions, respectively. Band intensities: s (strong); m (medium); w (weak). Key: (G) [Li⊂12-C-4][$CF_3SO_2N(CH_2)_3OCH_3$]; (H) [Li⊂15-C-5][$CF_3SO_2N(CH_2)_3OCH_3$]; (I) [Li⊂18-C-6][$CF_3SO_2N(CH_2)_3OCH_3$]; (J) [Li⊂2.1.1][$CF_3SO_2N(CH_2)_3OCH_3$]; (K) [Li⊂2.2.1][$CF_3SO_2N(CH_2)_3OCH_3$]; (L) [Li⊂2.2.2][$CF_3SO_2N(CH_2)_3OCH_3$].

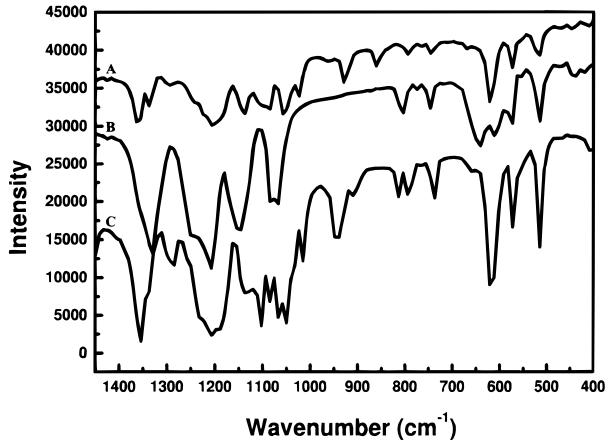

Figure 3. Representative FTIR spectra for Li[$(CF_3SO_2)_2N$] macrocycle complexes: (A) [Li⊂12-C-4][$(CF_3SO_2)_2N$]; (B) Li-[$(CF_3SO_2)_2N$]; (C) [Li⊂2.1.1][$(CF_3SO_2)_2N$].

sess more than one coordination environment of the lithium, resulting in a number of different complexes with different solid phases.

Upon complex formation of Li[$CF_3SO_2N(CH_2)_3OCH_3$] with cryptand macrocycles, the $\nu_{as}(SO_2)$ band shifts to lower wavenumbers (from 1277 to ∼1263 cm^{-1}) which contrasts with the shift to higher frequency (from 1277 to 1289, 1280 cm^{-1}) for the $\nu_{as}(SO_2)$ bands of the [Li⊂crown ether][$CF_3SO_2N(CH_2)_3OCH_3$] complexes. Furthermore, the $\nu_{as}(SO_2)$ bands of Li[$(CF_3SO_2)_2N$] shift to higher frequency upon complexation with cryptands and crown ethers. These observations suggest that cryptand macrocycles more effectively shield [$CF_3SO_2N(CH_2)_3OCH_3$]$^-$ from direct ion pairing with the lithium cation.

Ionic Conductivity. The temperature dependence of the ionic conductivity for amorphous polymer electrolytes was fit to the semiempirical Vogel−Tamman−Fulcher (VTF) function (eq 1), which is characteristic

$$\sigma = AT^{-0.5} \exp[-B/(T - T_o)] \quad (1)$$

of systems in which ion motion is coupled to motions of the viscous medium.[44−46] T_o is a parameter related to the glass transition temperature of the polymer salt complex ($T_o \sim T_g - 50$ °C), B is a pseudo-activation energy term related to the fluctuations in the electrolyte matrix that facilitate ion migration, and the preexponential factor, A, is dependent on the concentration of charge carriers in the matrix. By contrast, the conductivity data for the crystalline complexes may be fit to the Arrhenius equation, eq 2, which indicate that ions move by a simple hopping mechanism.

$$\sigma = A \exp[-E_a/RT] \quad (2)$$

The temperature-dependent ionic conductivity of the amorphous Li[$CF_3SO_2N(CH_2)_3OCH_3$] complexes fits the VTF relationship rather well, Figure 4, whereas the crystalline samples in the Li[$(CF_3SO_2)_2N$] samples are better fit by the Arrhenius equation, Figure 5. Table 7 indicates the fit of the T_o, B, and A terms of the VTF function to the temperature-dependent ionic conductivity of the amorphous Li[$CF_3SO_2N(CH_2)_3OCH_3$] complexes and the amorphous [Li⊂18-C-6][$(CF_3SO_2)_2N$] complex. The T_o term is fixed at 50 °C below the measured glass transition, and the amorphous sample with the lowest T_o value exhibits the highest ionic conductivity.

The data in Table 7 indicate a higher concentration of charge carriers for [Li⊂cryptand][$CF_3SO_2N(CH_2)_3OCH_3$] complexes than for [Li⊂crown ether][$CF_3SO_2N(CH_2)_3OCH_3$] complexes, and this may arise from strong coordination to the cation and more effective shielding of the cation by the cryptand macrocycle. [Li⊂cryptand]-[$CF_3SO_2N(CH_2)_3OCH_3$] complexes and [Li⊂crown ether]-[$CF_3SO_2N(CH_2)_3OCH_3$] display similar pseudo-activation energies. However, small decreases in the pseudo-

(44) Vogel, H. *Phys. Z.* **1921**, *22*, 645.
(45) Tamman, G.; Heese, W. *Z. Anorg. Allg. Chem.* **1926**, *156*, 245.
(46) Fulcher, G. S. *J. Am. Ceram. Soc.* **1925**, *8*, 339.

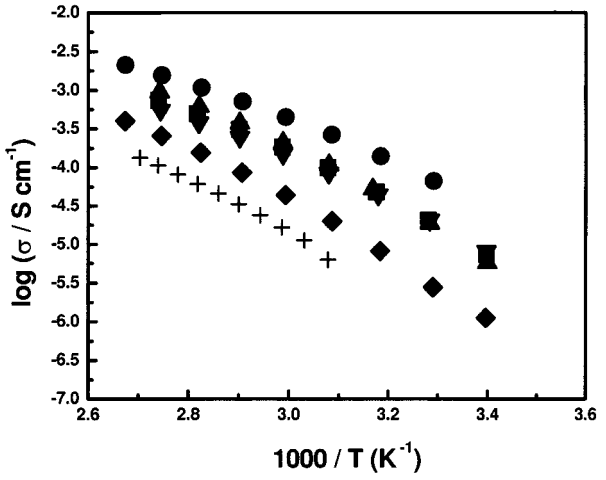

Figure 4. Temperature dependent conductivities (σ) of 1:1 ratios of [Li⊂2.2.2][$CF_3SO_2N(CH_2)_3OCH_3$] (■), [Li⊂2.2.1][$CF_3SO_2N(CH_2)_3OCH_3$] (●), [Li⊂2.2.1][$CF_3SO_2N(CH_2)_3OCH_3$] (▲), [Li⊂18-C-6][$CF_3SO_2N(CH_2)_3OCH_3$] (▼), [Li⊂15-C-5][$CF_3SO_2N(CH_2)_3OCH_3$] (◆), and [Li⊂12-C-4][$CF_3SO_2N(CH_2)_3OCH_3$] (+).

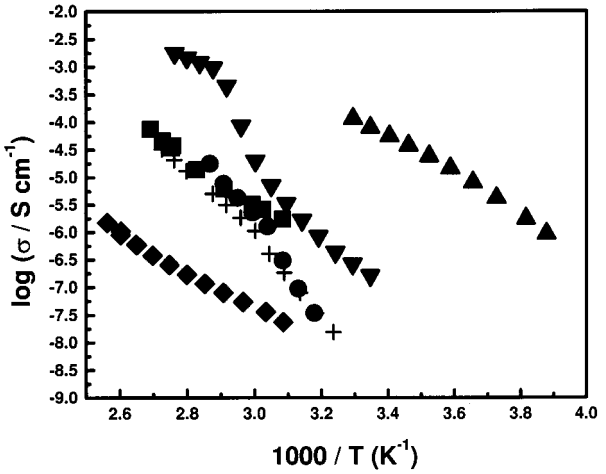

Figure 5. Temperature dependent conductivities (σ) of 1:1 ratios of [Li⊂12-C-4][$(CF_3SO_2)_2N$] (■), [Li⊂15-C-5][$(CF_3SO_2)_2N$] (●), [Li⊂18-C-6][$(CF_3SO_2)_2N$] (▲), [Li⊂2.1.1][$(CF_3SO_2)_2N$] (▼), [Li⊂2.2.1][$(CF_3SO_2)_2N$] (◆), and [Li⊂2.2.2][$(CF_3SO_2)_2N$] (+).

activation energy term from [Li⊂2.2.2][$CF_3SO_2N(CH_2)_3OCH_3$] to [Li⊂2.1.1][$CF_3SO_2N(CH_2)_3OCH_3$] may result from the energy required for the larger [Li⊂2.2.2] cation to diffuse in the amorphous electrolyte in comparison to the smaller [Li⊂2.2.1] and [Li⊂2.1.1] cations. Conversely, [Li⊂crown ether][$CF_3SO_2N(CH_2)_3OCH_3$] complexes exhibit an increase in the pseudo-activation term from the [Li⊂18-C-6][$CF_3SO_2N(CH_2)_3OCH_3$] complex to the [Li⊂12-C-4][$CF_3SO_2N(CH_2)_3OCH_3$] complex.

Table 7.. VTF Parameters for the Amorphous Complexes

complex	A (S K$^{1/2}$ cm^{-1})	B (K)	$T_g - 50 \approx T_o$ (K)
[Li⊂2.2.2][$CF_3SO_2N(CH_2)_3OCH_3$]	2.3	1422	173
[Li⊂2.2.1][$CF_3SO_2N(CH_2)_3OCH_3$]	2.3	1306	166
[Li⊂2.1.1][$CF_3SO_2N(CH_2)_3OCH_3$]	2.2	1263	188
[Li⊂18-C-6][$CF_3SO_2N(CH_2)_3OCH_3$]	0.5	1057	192
[Li⊂15-C-5][$CF_3SO_2N(CH_2)_3OCH_3$]	1.0	1249	197
[Li⊂12-C-4][$CF_3SO_2N(CH_2)_3OCH_3$]	0.6	1276	205
[Li⊂18-C-6][$(CF_3SO_2)_2N$]	2.9	1147	165

The VTF parameters indicate that the [Li⊂18-C-6][$(CF_3SO_2)_2N$] complex contains a larger concentration of charge carriers than the corresponding [Li⊂18-C-6][$CF_3SO_2N(CH_2)_3OCH_3$] complex. Apparently the more weakly basic $[(CF_3SO_2)_2N]^-$ results in a reduction of cation−anion interactions, and the concentration of charge carriers in [Li⊂18-C-6][$(CF_3SO_2)_2N$] is similar to the concentration of charge carriers in the weakly ion paired [Li⊂cryptand][$CF_3SO_2N(CH_2)_3OCH_3$] complexes.

Conclusions

Ionic glass formation is favored by a mismatch of the cation diameter and macrocycle cavity size for the Li[$CF_3SO_2N(CH_2)_3OCH_3$] complexes. Crystalline materials are observed for the complexes of Li[$(CF_3SO_2)_2N$], with the exception of [Li⊂18-C-6][$(CF_3SO_2)_2N$]. Spectroscopic evidence indicate significant differences between Li[$CF_3SO_2N(CH_2)_3OCH_3$] cryptand and Li[$CF_3SO_2N(CH_2)_3OCH_3$] crown ether complexes, whereas the spectra of cryptand and crown ether complexes of Li[$(CF_3SO_2)_2N$] are similar. These observations are consistent with the basicity of the anions ($[CF_3SO_2N(CH_2)_3OCH_3]^-$ > $[(CF_3SO_2)_2N]^-$). The irregularity and ether oxygen substituent of $[CF_3SO_2N(CH_2)_3OCH_3]^-$ appears to favor glass formation, whereas the more symmetrical $[(CF_3SO_2)_2N]^-$ favors crystalline phases for the Li[$(CF_3SO_2)_2N$] complexes. This observation is supported by the difference in thermal properties between the Li[$CF_3SO_2N(CH_2)_3OCH_3$] and K[$CF_3SO_2N(CH_2)_3OCH_3$] salts and the similarity between the thermal properties of the Li[$(CF_3SO_2)_2N$] and K[$(CF_3SO_2)_2N$] salts.

Acknowledgment. This work was supported by the MRSEC program of the National Science Foundation (DMR-9632472) at the Materials Research Center of Northwestern University.

CM990376F